Use of Novel Adaptive Digital Feedback for Magnetic Measurements Under Controlled Magnetizing Conditions

Stan Zurek, Philip Marketos, Turgut Meydan, and Anthony J. Moses

Wolfson Centre for Magnetics Technology, School of Engineering, Cardiff University, Cardiff CF24 3AA, U.K.

There are increasing calls to employ conventional magnetic testers, such as the Epstein frame and single sheet tester, for the accurate measurements of magnetic properties of soft magnetic materials under fully controlled nonsinusoidal flux density waveforms. This paper presents a computerized automated adaptive digital feedback system built for that purpose. We present several examples of the ability of the system to control an arbitrary shape of the flux density waveforms over the frequency range of the data acquisition system (0.5 Hz to 2 kHz) and for peak flux density up to 90% of saturation. The control algorithm is capable of magnetizing magnetic material under controlled sinusoidal, triangular, trapezoidal, and pulsewidth-modulated magnetizing conditions as well as other arbitrary waveforms that do not contain dc components. We provide a full description of the adaptive digital feedback technique together with measurements showing the B–H loops for several magnetic materials under various controlled excitation conditions.

***Index Terms*—Digital feedback, magnetic measurement, power loss measurement, rotational magnetization, two-dimensional magnetization, waveform control.**

I. Introduction

INTERNATIONAL standards for magnetic measurements of power loss in electrical steels state that power loss measurements are taken only provided that the shape of the flux density waveform, B, remains sinusoidal with respect to time [1]. Since systems involving testing of soft magnetic materials are in general nonlinear, negative feedback must be used to keep the flux density sinusoidal at all times.

For traditional measurements, an analog electronic circuit (Fig. 1) usually provides sufficient control of the shape of the flux density waveform. However, when there is a need for nonstandard testing, e.g., very high flux density, magnetic material with very high permeability, or two-dimensional magnetization conditions, these systems fail either due to nonsufficient control or due to oscillations in the feedback loop. There is no universal solution to this problem in control theory [2], [3].

Because of continuing progress in computer technology, digital systems have, over the past 20 years, began to compete successfully and take over from analog circuits in many applications. Most of the current measurement devices include a digital microprocessor, and rapid development of programming languages allows the use of computer-based systems in more user-friendly and versatile ways [4], [5].

One of the most important limitations of analog feedback is the oscillation of the magnitude of the controlled signal. This phenomenon occurs when the gain of the feedback is too high, which leads to instability of the closed control loop. In general, iterative digital feedback does not have to be a real-time process and iterations can be carried out practically off-line. Therefore, the dynamics of single iteration are not critical to the stability of the control algorithm [6]–[8]. This, combined with the robustness given by the software, provides excellent conditions for achieving controlled excitation when carrying out magnetic measurements.

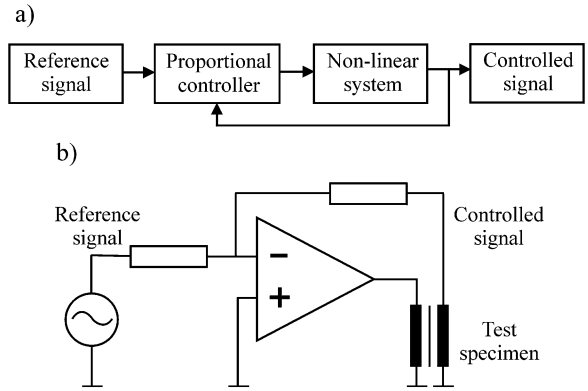

Fig. 1. Analog electronic feedback: (a) block diagram, and (b) simplified electronic circuit.

Since the B–H characteristics of soft magnetic materials are highly nonlinear, the prediction of the material behavior under uncontrolled excitation conditions is very difficult. The simplest way of achieving the desired wave shape of B, for example sinusoidal, is by iteratively modifying the magnetizing current. Some analog techniques can be helpful in shortening the control process, but they are not universally applicable, and usually require additional data about the magnetizing system whereas the main concept of iterative feedback remains the same [9], [10]. The problem of maintaining a controlled flux density becomes even more challenging in the case of unconventionally shaped magnetizing yokes, magnetic materials with high permeability, and magnetic circuits containing inhomogeneous air gaps.

In this paper, a novel digital feedback algorithm is described. All necessary feedback parameters and coefficients are computed during the control process with no requirement of prior knowledge of the magnetizing system (e.g., yoke dimensions, inductance of windings, etc.). The algorithm is fully adaptive and can be used with a range of magnetizing systems providing

Digital Object Identifier 10.1109/TMAG.2005.854438

that the excitation waveform does not contain a dc component, as will be explained in the following sections.

II. The Idea of Adaptive Digital Feedback for Alternating Magnetization

The block diagram of the digital feedback system used for the control of the magnetization waveform is presented in Fig. 2. A computer, with virtual instrumentation software (LabVIEW) and a data acquisition and generation card (DAQ) generates a voltage waveform. This waveform is fed through a low-pass filter (LPF) to a power amplifier (PA). An isolating transformer (IT) removes any dc component in the magnetizing current. The magnetizing current is fed to a magnetizing yoke through a shunt resistor, which allows current measurement. All measured signals are connected to the inputs of the DAQ, from where they are acquired by the software.

The feedback algorithm presented here is called "digital" because all the operations: low-pass filtering, integration, differentiation, Fourier transform, and proportional controller, are implemented in the software. No external signal conditioning or analog signal processing is used.

The digital feedback algorithm consists of four main parts (Fig. 3). The first is the measuring thread ($\mathbf{A}$ in Fig. 3), in which acquired signals are used to calculate the flux density, $\boldsymbol{B}$ [T], magnetic field strength, $\boldsymbol{H}$ [A/m], power loss per unit mass P [W/kg], etc. (The bold italic symbols: $\boldsymbol{B}, \boldsymbol{H}, \boldsymbol{I}$, etc. denote one-dimensional arrays of data, which represent the corresponding waveforms.)

The second thread ($\mathbf{B}$ in Fig. 3) is responsible only for digital feedback. The same input data are used as for the measuring thread. However, additional calculations are implemented, such as digital filtering and computation of the relative difference between reference waveform and real $\boldsymbol{B}$

$$\mathbf{Diff}_{(i)} = (\boldsymbol{B}_{\mathbf{ref}} - \boldsymbol{B}_{\mathbf{real}(i)})/B_{\mathrm{ref}} \tag{1}$$

where

- $\mathbf{Diff}$ waveform of relative difference between reference and real waveforms;
- $\boldsymbol{B}_{\mathbf{ref}}$ reference (ideal) flux density waveform;
- $\boldsymbol{B}_{\mathbf{real}}$ real (measured) flux density waveform;
- B_{ref} peak value of reference flux density waveform;
- i present iteration.

(The $\boldsymbol{B}_{\mathbf{ref}}$ and B_{ref} remain constant during the control process, therefore they are not indexed.)

In each iteration, the waveform $\mathbf{Diff}_{(i)}$ is used to modify the generated output voltage waveform accordingly ($\mathbf{C}$ in Fig. 3), until the difference between the reference and real waveform is equal or less than the user defined value.

The algorithm initially assumes that $\boldsymbol{B}$ depends linearly on the magnetizing current $\boldsymbol{I}$. The nonlinearity between measured $\boldsymbol{B}$ and applied $\boldsymbol{H}$ or magnetizing current $\boldsymbol{I}$ is very complicated and strongly dependent on the shape and magnetic properties of the yoke and the specimen. The passive LPF and PA introduce a phase lag up to several tens of degrees for different harmonics. The phase lead/lag functions of the LPF and the PA can be found relatively easily (see Fig. 4), but the magnetizing yoke, the random air gaps as well as the B–H characteristics of the specimen cause the transfer function of the whole system to continually change. In order to compensate for this, a module that

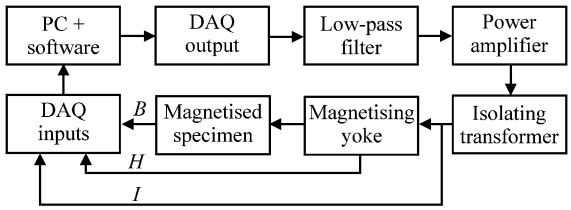

Fig. 2. Block diagram of digital feedback system.

calculates the phase lead/lag between the output voltage generated by the DAQ and actual magnetizing current for each harmonic is implemented ($\mathbf{D}$ in Fig. 3). The array of phase shifts for all harmonics is continuously adapted in every subsequent iteration. Before the DAQ generates the output voltage, the waveform computed by the proportional controller ($\mathbf{C}$ in Fig. 3) is fed to the *Correct phase* element (see $\mathbf{D}$ in Fig. 3), which provides a Fourier transform of the waveform, modifies the phase of each harmonic, and then calculates an inverse Fourier transform.

This artificially "distorted" voltage output waveform is then generated by the DAQ and "converted" through the nonlinear components (LPF, PA, IT, yoke, and specimen) to the desired shape of the flux density waveform.

As the permeability of the sample under investigation usually changes very rapidly throughout the magnetization cycle, a greater modification of the controlled signal than predicted by the feedback may occur in some regions of the magnetizing curve. This would lead to oscillations of the magnitude of the controlled waveform. In practice, feedback gains equal to 0.3 or less successfully prevent this (these are shown as *Gain* and *Angle Gain* icons in $\mathbf{C}$ and $\mathbf{D}$ in Fig. 3, respectively).

Since in general (taking into consideration the staircase effect [11]) the DAQ acquires a different number of points per magnetization cycle than it generates, there is a module responsible for rendering the waveform to another number of points (this is shown as *Change points* icon in Fig. 3). A simplified block diagram of the adaptive digital feedback system is presented in Fig. 5.

The equation for calculating the output voltage waveform in subsequent iterations takes a form

$$\mathbf{Out}_{(i)} = \mathbf{F}_{(i)}\left(\mathbf{Out}'_{(i)}\right) \tag{2}$$

where

- i present iteration;
- $\mathbf{Out}$ voltage waveform generated by the DAQ.

$\mathbf{Out}'$ is the output waveform calculated for ith iteration by the proportional controller as

$$\mathbf{Out}'_{(i)} = \mathbf{Out}_{(i-1)} + G \cdot \left|\mathbf{Out}_{(i-1)}\right| \cdot \mathbf{Diff}_{(i)} \tag{3}$$

where

- G gain of the proportional controller (shown as *Gain* icon in $\mathbf{C}$ in Fig. 3);
- $\mathbf{Diff}$ difference waveform calculated according to (1);
- $i-1$ previous iteration.

The waveform $\mathbf{Out}'_{(i)}$ from (3) is a one period of continuous function and can also be expressed as a finite Fourier series for given iteration

$$\mathbf{Out}'_{(i)} = \sum_{k=1} \left[A_{(k)} \cdot \cos\left(k \cdot 2 \cdot \pi \cdot f \cdot t + \phi_{(k)}\right)\right]_{(i)} \tag{4}$$

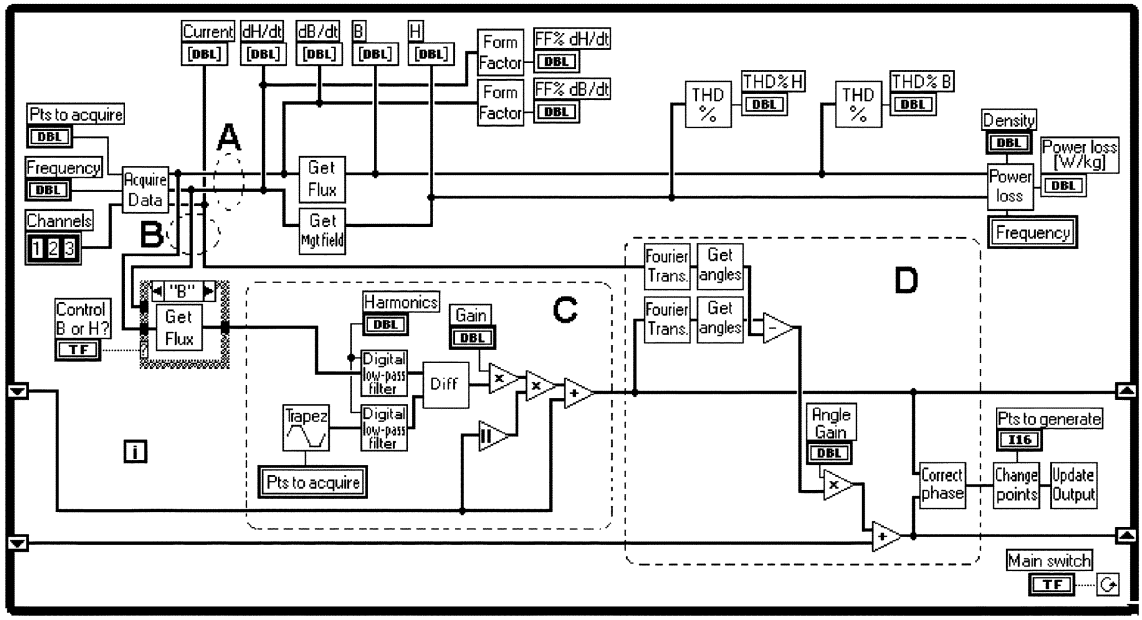

Fig. 3. Simplified adaptive digital feedback algorithm written in LabVIEW (not all modules are shown): A—measurement thread, B—control thread, C—proportional controller, D—adaptation module.

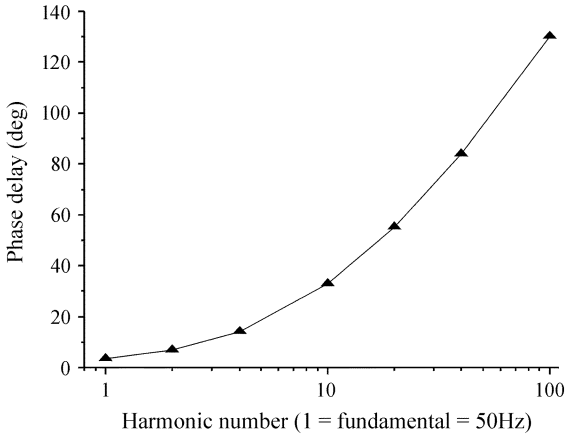

Fig. 4. Typical phase lag function for harmonics spectrum for low-pass passive RC filter (R = 2 k, C = 10 nF) and power amplifier MT2400.

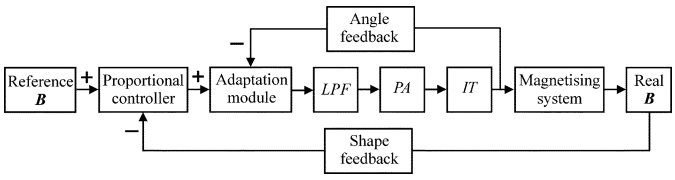

Fig. 5. Block diagram of digital adaptive feedback system.

where

- k harmonic number;
- A magnitude of the kth harmonic;
- f magnetizing frequency;
- t time;
- φ phase shift of the kth harmonic.

Symbol $\boldsymbol{F}_{(i)}$ in (2) denotes a function of phase lead/lag for all harmonics for given iteration. It is applied by module *Correct phase* in **D** in Fig. 3 as

$$\mathbf{Out}_{(i)} = \sum_{k=1} \left[A_{(k)} \cdot \cos\left(k \cdot 2 \cdot \pi \cdot f \cdot t + \varphi_{(k)} + \alpha_{(k)}\right)\right]_{(i)} \tag{5}$$

where $\alpha_{(k)}$ is the phase lead/lag of the kth harmonic calculated for each iteration as

$$\alpha_{(k,i)} = \alpha_{(k,i-1)} + G_\alpha \cdot \left(\alpha_{B(k,i)} - \alpha_{I_{(k,i)}}\right) \tag{6}$$

where

- G_α gain of angle feedback (shown as *Angle Gain* icon in **D** in Fig. 3);
- α_B phase of the kth harmonic of flux density waveform;
- α_I phase of the kth harmonic of magnetizing current.

Hence, the array of phase shifts for all harmonics which is fed to the module *Correct phase* can be written for given iteration as

$$\boldsymbol{\alpha}_{(i)} = \left[\alpha_{1(i)}, \alpha_{2(i)}, \ldots, \alpha_{n(i)}\right] \tag{7}$$

where

- $\boldsymbol{\alpha}$ array of phase shifts for all analyzed harmonics;
- α phase shift for a given harmonic;
- n total number of analyzed harmonics.

III. Adaptive Digital Feedback for Two- and Three-Channel Magnetizing Conditions

The adaptive digital feedback described above can be used also for more complex magnetizing conditions, namely, when more than one magnetizing current produces the magnetizing field. Examples of such systems are two-dimensional (2-D)

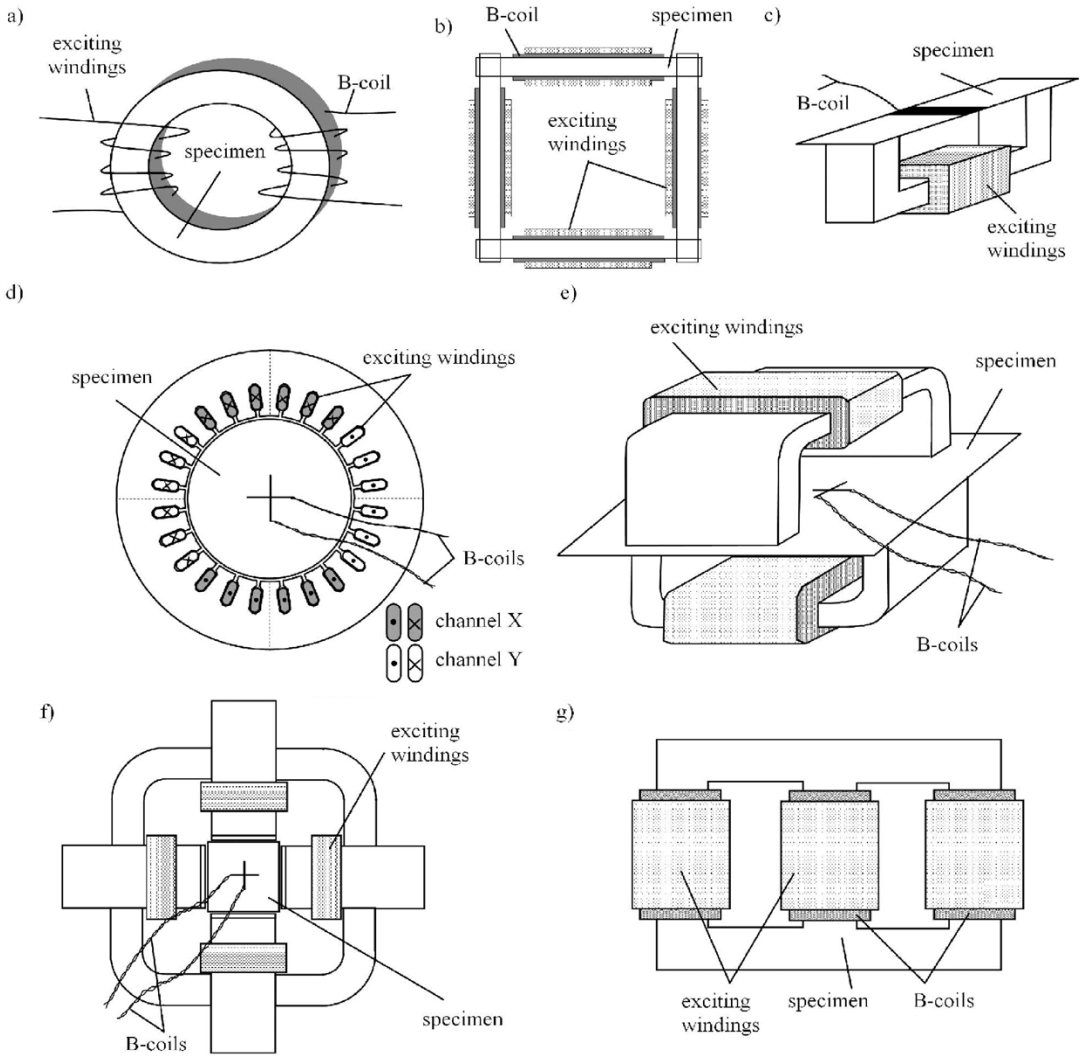

Fig. 6. Types of magnetizing testers used in investigation: (a) toroid, (b) Epstein frame, (c) single strip tester, (d) round 2-D yoke, (e) double-sided 2-D yoke, (f) planar 2-D yoke, and (g) small three-phase transformer.

magnetizing yokes and three-phase transformers. Measurements under such magnetizing conditions are more difficult to carry out due to the complex dependence of the components of magnetizing field on each other. In 2-D systems, the magnetizing field is composed of two orthogonal magnetic components [see also Fig. 6(d)–(f)]. Arbitrary magnetizing conditions can be achieved as a result of appropriate change in magnitude, phase, or shape of these two components in X and Y directions [9], [10], [12], [13]. For example, if both components are set to be sinusoidal the resultant field is elliptical, and the shape of the ellipse depends on the magnitude and phase of both components.

The digital feedback described in the previous section is fully adaptive and can be used for waveform control under 2-D and three-phase excitation. The concept remains the same as for alternating magnetization. The only difference is the use of as many control threads, as there are magnetizing channels instead of one. In practice, this means that the control thread and adaptation module ($\mathbf{B}$, $\mathbf{C}$, and $\mathbf{D}$ in Fig. 3) are simply doubled for all the magnetizing channels. Naturally, there is a need for measuring more signals as appropriate, in order to have independent information about B–I relationship for each magnetizing channel.

The algorithm calculates the shape of the waveform in each magnetizing channel independently. If the magnetic material is anisotropic there is an influence of waveforms in one channel to the next (due to magnetics). In each iteration, the shape of the waveform in a given channel is compared to the reference waveform, so as to achieve the desired shape. Therefore, during the control process such interdependencies of the shape of the waveforms are continuously and automatically corrected. This makes the feedback "adaptive," since there is no need to know how the magnetizing channels interact with each other.

IV. Results

Three DAQs were used for generation and acquisition of signals: NI PCI-6052E [14], NI PCI-4452 [15], and NI PCI-6711E [16] (generation only), all supplied by National Instruments. An LPF simple passive RC circuit, with user defined cutoff frequency, was designed and used. It was suggested in [11] that the magnetic measurements could be carried out with no LPF present so this was also tested. If the numbers of generated and

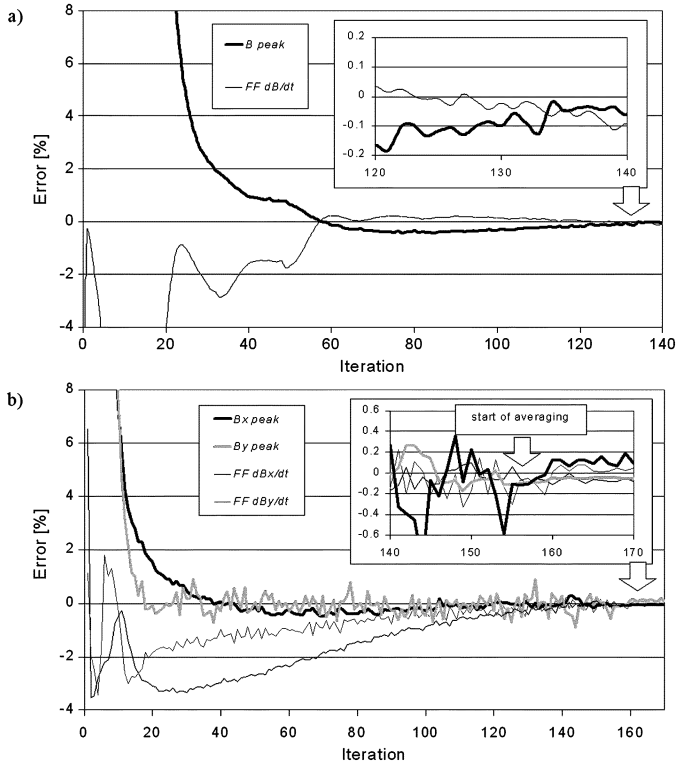

Fig. 7. Typical graphs of the performance of the adaptive digital feedback: (a) alternating magnetization at 1 kHz, 1.6 T, conventional nonoriented electrical steel sheet, and (b) 2-D rotational magnetization at 50 Hz, 1.5 T, conventional grain-oriented electrical steel. (The insets show the magnifications of the final part of controlling process. The inset in (b) shows the influence of averaging of the readings from 25 periods.)

TABLE I
TYPICAL VALUES OF CONVERGENCE TIME FOR ALTERNATING AND ROTATIONAL MAGNETIZATION

	Conventional grain-oriented electrical steel				Conventional non-oriented electrical steel			
	Epstein frame		*2D* yoke		Epstein frame		*2D* yoke	
Frequency [Hz]	Time [min]	B_{peak} [T]	Time [min]	B_{rot} [T]	Time [min]	B_{peak} [T]	Time [min]	B_{rot} [T]
1	20	1.9	40	1.3	8	1.6	10	1.5
5	6	1.9	10	1.3	2	1.6	2	1.5
50	1	1.9	1	1.5	<1	1.6	<1	1.7
1000	<1	1.9	<0.5	1.0	<0.5	1.6	<0.5	1.0

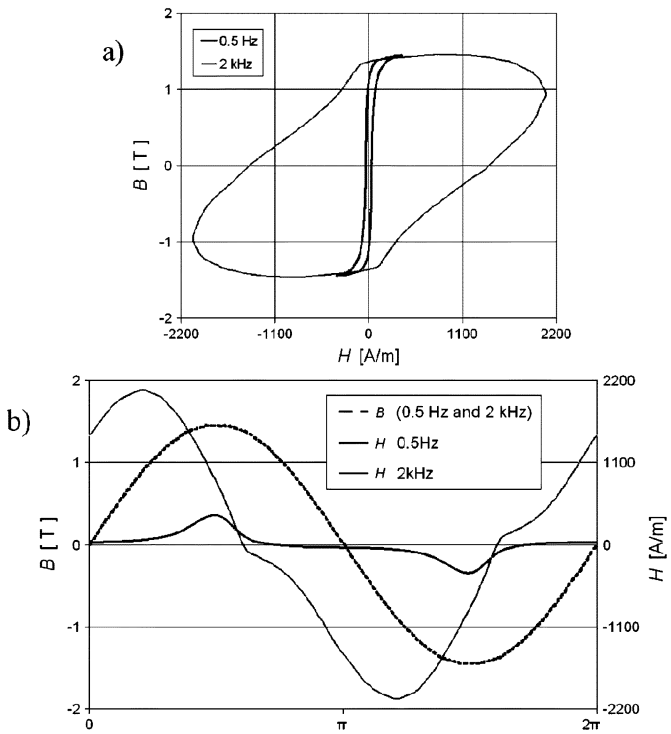

Fig. 8. Conventional 0.5 mm thick nonoriented low silicon electrical steel magnetized in an Epstein frame at 0.5 Hz and 2 kHz, 1.46 T: (a) B–H loops, and (b) corresponding waveforms of B (sinusoidal-controlled) and H.

acquired points were not equal (condition suggested in [11]), the LPF would not be necessary.

Current mode power amplifiers, Crown MT2400 [17], were used as a power source with isolating transformers in order to remove any dc bias from their output currents. The magnetizing current waveform was found from the voltage waveform across the terminals of a shunt resistor.

Several magnetizing systems were used to test the versatility of the control algorithm (Fig. 6). These were: toroid, a conventional Epstein frame, a nonstandard single strip tester, various 2-D yokes, and a three-phase transformer. In all of these cases, the adaptive digital feedback proved to be stable.

Data processing can only be carried out once a complete cycle of the magnetizing waveform has been acquired. Therefore, the time of each iteration and thus the convergence time depend on the magnetizing frequency. As the frequency decreases the time of the cycle grows accordingly, but the number of iterations necessary to achieve a controlled state of magnetization remains approximately the same (see Fig. 7).

The convergence time is higher not only due to the length of the period, but also because of the large amount of data that is being processed. To maintain the accuracy of the measurement, the number of points per period must increase at low frequencies. (This is dictated by the minimum sampling frequency of the DAQ [14]–[16] and also by the fact that for lower number of points the staircase effect [11] is more pronounced.) Consequently, the processing power needed to carry out the Fourier transform grows exponentially. For this reason, a controlled excitation for frequencies below 0.5 Hz would take several hours to approach the required conditions.

Fig. 7 presents typical graphs of adaptive digital feedback performance. The feedback starts from zero waveforms, so all the factors have initially 100% error (peak value of flux density—thick line, and percentage error of the form factor—thin line). As the software processes subsequent iterations these factors decrease to zero.

It can be seen that the percentage error of the form factor, FF, of dB/dt is well within the limits specified by the international standard for magnetic measurements [1] and also the percentage error of B_{peak} is within 0.2% of the ideal value.

The accuracy of the measurement can be improved by using the averaging of the readings [Fig. 7(b)], but again it affects the controlling time. Nevertheless, even as low as 0.5 Hz result has been measured for alternating magnetization. The highest magnetizing frequency at which the samples were tested was

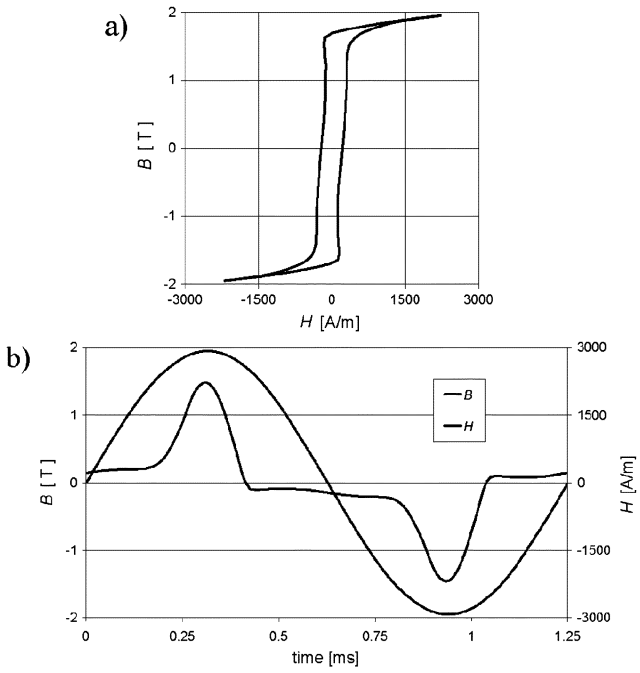

Fig. 9. Conventional 0.27 mm thick grain-oriented 3% silicon electrical steel magnetized in an Epstein frame at 800 Hz, 1.95 T: (a) B–H loop, and (b) corresponding waveforms of B (sinusoidal-controlled) and H.

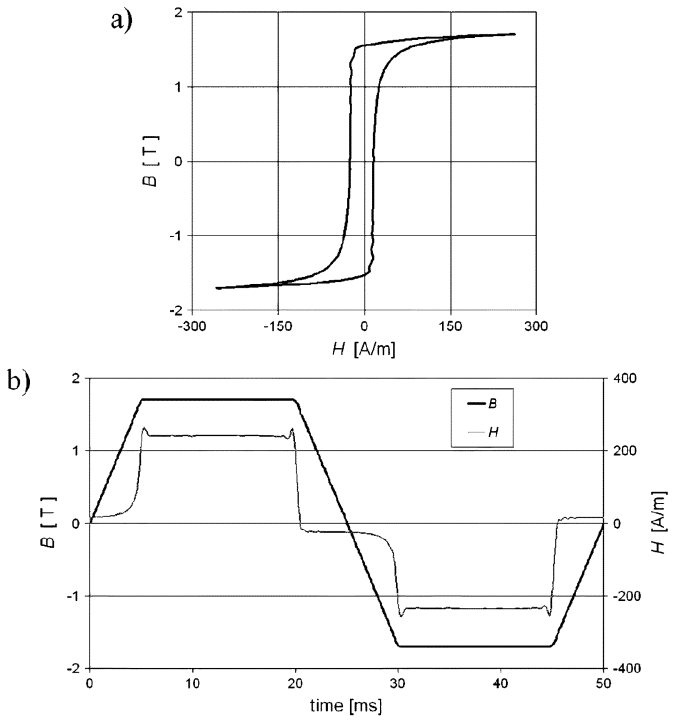

Fig. 10. Conventional 0.27 mm thick grain-oriented 3% silicon electrical steel magnetized in Epstein frame at 20 Hz, $B_{\rm peak} = 1.70$ T: (a) B–H loop, and (b) corresponding waveforms of B (trapezoidal-controlled) and H.

2 kHz and it was limited mainly by the sampling frequency of the DAQ, which for NI PCI-4452 is 200 000 samples per second. The authors believe that the algorithm would work as intended even for higher frequencies.

Typical values of the convergence time for an Epstein frame [Fig. 6(b)] and a 2-D yoke [Fig. 6(f)] are presented in Table I. In each case, the magnetization started from zero and was gradually controlled until $B_{\rm peak}$ (in alternating unidirectional magnetization) or $B_{X\rm peak}$ and $B_{Y\rm peak}$ (orthogonal B components in rotational magnetization) reached a satisfactory level of control.

The times presented in Table I are satisfactory for the frequencies above 5 Hz. However, for lower frequencies they are very slow and might be not acceptable for some measurements.

To speed up the control process, other techniques may be used [9], [10]. In particular, controlling time can be reduced by using prerecorded controlled measurement. In such a case the feedback does not start from a zero level, which allows the convergence time to be reduced to a few periods of the given magnetizing frequency.

The described adaptive digital feedback algorithm can be used to provide control for arbitrary waveform of flux density, such as sinusoidal, triangular, trapezoidal, pulsewidth modulation (PWM), etc., provided they do not contain a dc component. The IT prevents the dc component of the current waveform to reach the magnetizing setup. This is a desired condition as the dc-biased magnetizing current would alter the magnetization conditions.

There are two limitations. Since, in practice only lower order harmonics significantly affect the shape of flux density waveform, a low-pass filter is placed in the control thread to improve the speed of data processing and the stability of the feedback. The reference waveform is preprocessed in the same manner (see **C** in Fig. 3), so consequently it is possible to control only a waveform, which can be expressed by a finite Fourier harmonic series. For nonsinusoidal waveforms, the number of harmonics can be increased to provide better representation of the ideal signal. However, because the Fourier transform can decompose/compose only mathematically continuous functions, it is impossible to fully apply it to the waveforms with local discontinuity due to the Gibbs phenomenon [18]. The second problem arises from the performance of the PA, since it is extremely difficult to drive fast rising current into an inductor. For that reason, it is physically impossible to generate square-shaped current waveform even without feedback. Hence, the rise time of the output current sets the limits to the shape and frequency of the controlled signal.

In practice, under alternating magnetization conditions, typically no more than 50 harmonics are sufficient to provide an acceptable level of control for commonly used nonoriented and grain-oriented electrical steel and would be similar to other commercial soft magnetic materials. Under rotational conditions, magnetization of grain-oriented steel is extremely difficult to control, due to its high anisotropy, and sometimes up to 150 harmonics might be required.

Fig. 8 shows the results obtained for testing conventional nonoriented electrical steel in the Epstein frame at 0.5 Hz and 2 kHz. In both cases, the shape of flux density waveform has been controlled to be sinusoidal with $B_{\rm peak} = 1.46$ T. The B waveforms presented in Fig. 8(b) are identical, thus only one curve is shown (dashed, black colored). Obviously the waveforms in Fig. 8(b) have different times of duration, 2000 ms for 0.5 Hz and 0.5 ms for 2 kHz, therefore they are plotted with respect to the magnetizing cycle.

Fig. 9 presents results of measurement made on conventional grain-oriented material in an Epstein frame at 800 Hz at flux

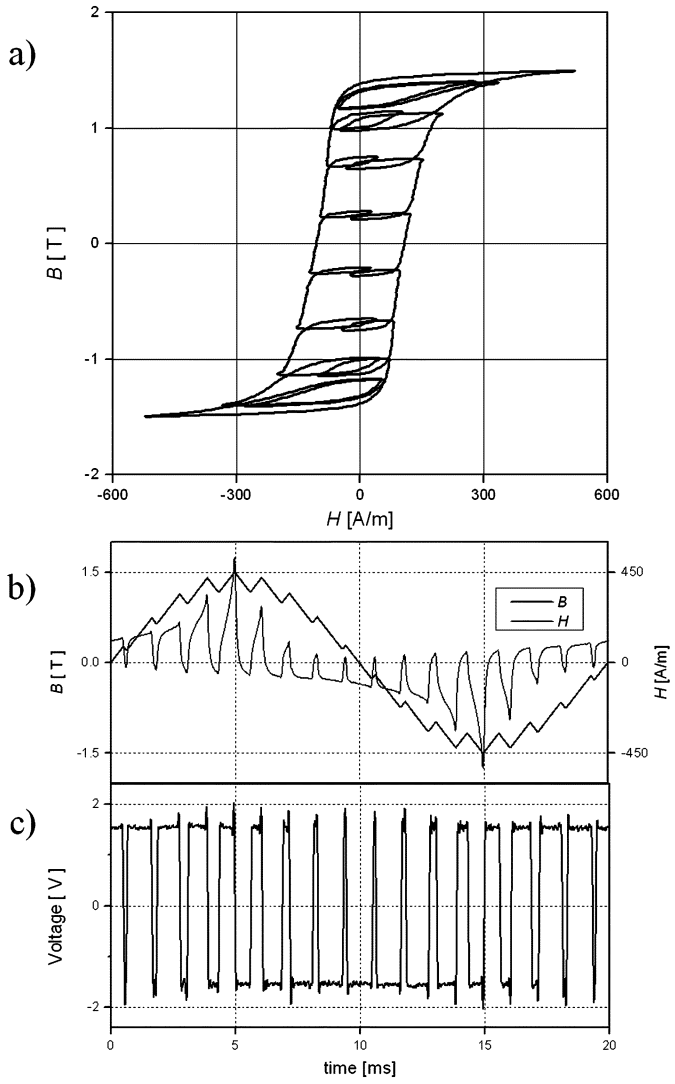

Fig. 11. Conventional 0.5 mm thick nonoriented low silicon electrical steel magnetized in Epstein frame at 50 Hz, $B_{\rm peak} = 1.50$ T: (a) B–H loop, (b) corresponding waveforms of B (PWM-controlled) and H, and (c) voltage waveform proportional do dB/dt.

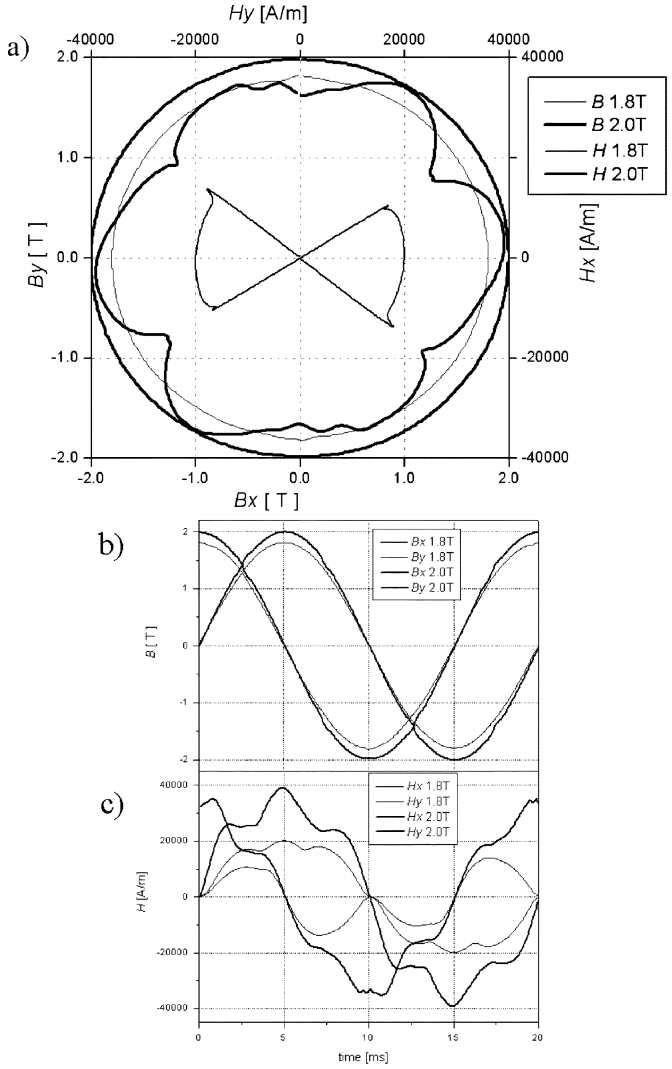

Fig. 12. Conventional 0.27 mm thick grain-oriented 3% silicon electrical steel magnetized in 2D yoke at 50 Hz, 1.80 T, and 2.00 T: (a) loci of B (circular-controlled) and H vectors, (b) corresponding B components, and (c) corresponding H components.

density $B_{\rm peak} = 1.95$ T. The B waveform is controlled to be sinusoidal.

Fig. 10 presents the results of measurements made on conventional grain-oriented material at 20 Hz using the Epstein frame. The shape of flux density waveform has been controlled to be trapezoidal with $B_{\rm peak} = 1.70$ T. The rise time is equal to 10% of the magnetizing cycle.

An example of a flux density waveform controlled to a typical PWM shape with local minima is shown in Fig. 11. The results are acquired for conventional nonoriented electrical steel magnetized in the Epstein frame at a fundamental frequency of 50 Hz with $B_{\rm peak} = 1.50$ T. The PWM waveform is modulated from a two-level signal with 18 pulses and index modulation $m = 0.8$.

The example presented in Fig. 12 is obtained using a round 2-D yoke [Fig. 6(d)] at 50 Hz for conventional grain-oriented, 3% silicon electrical steel. Rotational magnetization is controlled to be circular with the radius $B_{\rm rot} = 1.80$ T and 2.00 T within 1%. Those are believed to be some of the best high flux density results reported to date.

Fig. 13 demonstrates the ability of the adaptive digital feedback to control asymmetrical waveforms. The measurements were made on conventional nonoriented electrical steel magnetized at 50 Hz in a square 2-D yoke [Fig. 6(f)] under arbitrary 2-D conditions. The resultant loci of the B vector presented in Fig. 13(a) have complex shapes and are obtained by controlling the component B_X to be asymmetrically triangular and component B_Y to be symmetrically trapezoidal [Fig. 13(b)]. The resultant H waveforms are presented in Fig. 13(c).

The presented feedback also is capable of controlling an arbitrary waveform of magnetic field strength [19].

V. Conclusion

A novel adaptive digital feedback system has been described for use in making magnetic measurements on soft magnetic materials under defined and controlled magnetizing conditions.

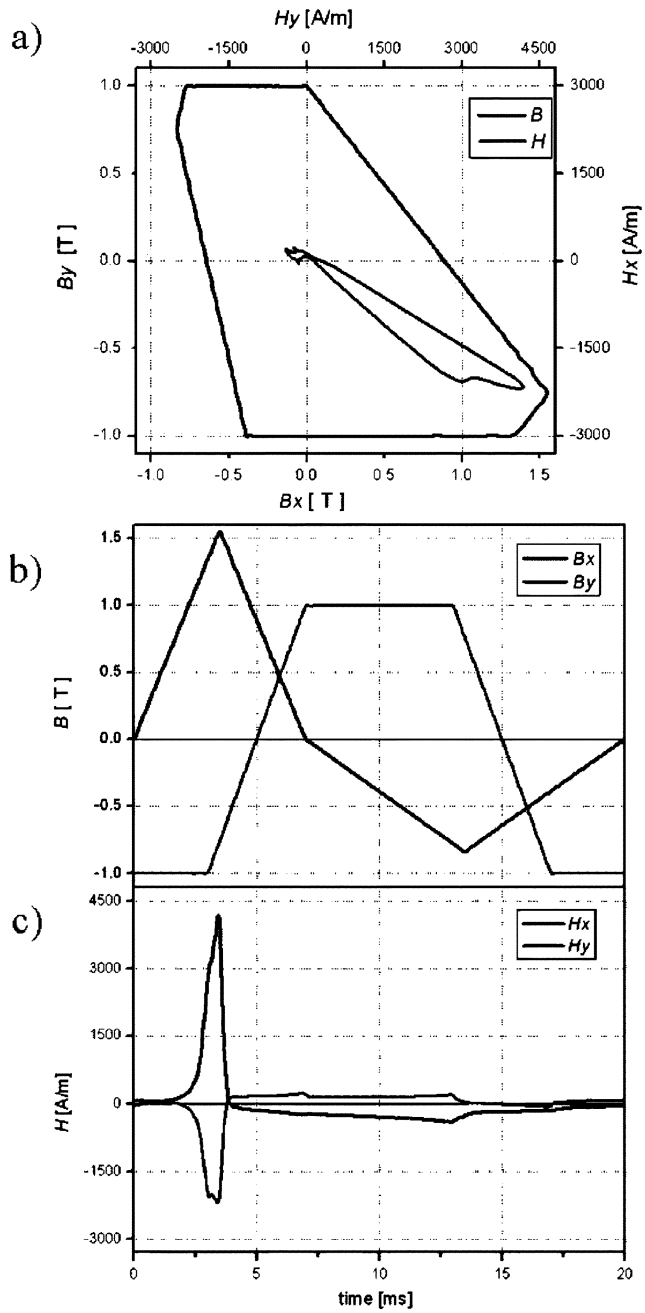

Fig. 13. Conventional nonoriented, low silicon electrical steel, 0.5 mm thick, magnetized under arbitrary 2-D conditions at 50 Hz: (a) loci of B (controlled) and H vectors, (b) corresponding waveforms of B_X (asymmetrical triangular) and B_Y (symmetrical trapezoidal), and (c) corresponding waveforms of H_X and H_Y.

Due to high stability and capability of adaptation to various magnetizing systems the novel adaptive digital feedback approach presents an excellent alternative to other types of digital feedback.

The algorithm is capable of achieving results for sinusoidal magnetization over a wide frequency range from 0.5 to 2000 Hz and with an error of magnitude of flux density, B, below 0.1% and error of form factor of dB/dt below 1.0%. Arbitrary shapes of flux density and magnetic field strength can be controlled with similar precision.

The controlling time at lower frequencies is considerably long and other techniques may be easily used in conjunction with the proposed algorithm, to shorten the process down to a few cycles of magnetizing frequency for a particular type of magnetizing yoke or measurement.

ACKNOWLEDGMENT

This work was supported by the EPSRC Grant GR/M95028/01 and EPSRC Platform Grant GR/R10493/01. The authors thank Dr R. Rygal (Czestochowa University of Technology, Poland) for valuable discussions during the development of this algorithm.

REFERENCES

[1] *Part 2 Methods of Measurement of the Magnetic Properties of Electrical Steels Sheet and Strip by Means of an Epstein Frame*, 1992. International Electrotechnical Commission IEC 404-2.

[2] W. Bolton, *Control Engineering*, 2nd ed: Longman, 1998, pp. 236–238.

[3] R. H. Bishop, *Modern Control Systems Analysis and Design Using MATLAB®*. Reading, MA: Addison Wesley, 1993, p. 152.

[4] A. Nafalski, T. Doan, and O. Gol, "Application of a virtual instrument concept in magnetic measurements," *J. Magn. Magn. Mater.*, vol. 160, pp. 154–156, 1996.

[5] N. Derebasi, R. Rygal, A. J. Moses, and D. Fox, "A novel system for rapid measurement of high-frequency magnetic properties of toroidal cores of different sizes," *J. Magn. Magn. Mater.*, vol. 215–216, pp. 684–686, 2000.

[6] N. Grote *et al.*, "Measurement of the magnetic properties of soft magnetic material using digital real-time current control," in *Non-linear Electromagnetic Systems*, V. Kose and J. Sievert, Eds. Amsterdam, The Netherlands: IOS Press, 1998, pp. 566–569.

[7] S. Bennett, *Real-Time Computer Control: An Introduction*. Englewood Cliffs, NJ: Prentice-Hall, 1988.

[8] A. Platil, P. Ripka, P. Kaspar, and J. Roztocil, "Sampling measurements with digital hysteresisgraph," *J. Magn. Magn. Mater.*, vol. 254–255, pp. 108–110, 2003.

[9] S. A. Spornic, A. Kedous-Lebouc, and B. Cornut, "Numerical waveform control for rotational single sheet testers," *J. Phys. IV*, pp. 741–744, 1998.

[10] D. Makaveev, J. Maes, and J. Melkebeek, "Controlled circular magnetization of electrical steel in rotational single sheet testers," *IEEE Trans. Magn.*, vol. 37, no. 4, pp. 2740–2742, Jul. 2001.

[11] K. Matsubara *et al.*, "Effect of staircase output voltage waveform of a D/A converter on iron losses measured using an H coil," *J. Magn. Magn. Mater.*, vol. 160, pp. 185–186, 1996.

[12] Y. Alinejad-Beromi, A. J. Moses, and T. Meydan, "New aspects of rotational field and flux measurement in electrical steel," *J. Magn. Magn. Mater.*, vol. 112, no. 1–3, pp. 135–138, 1992.

[13] S. Zurek and T. Meydan, "Digital feedback controlled RSST system," in *Proc. 16th SMM Conf.*, Dusseldorf, Germany, Sep. 2003.

[14] *DAQ PCI-6052E/6053E User Manual*, 1999. National Instruments, Multifunction I/O Board for PCI/PXI/1394 Bus Computers.

[15] *DAQ PCI-4451/4452 User Manual*, 1998. Dynamic Signal Acquisition Device for PCI, National Instruments.

[16] *DAQ PCI/PXI-6711/6713 User Manual*, 1998. National Instruments, Analog Voltage Output Device for PCI/PXI/CompactPCI.

[17] *Micro-Tech®, Analogue/Crown MT600, MT1200, MT2400 Power Amplifiers, Reference Manual*, 2001. Analogue Associates Ltd.

[18] E. P. Cunningham, *Digital Filtering: An Introduction*. Boston, MA: Houghton Mifflin, 1992, pp. 273–276.

[19] S. Zurek, P. Marketos, and T. Meydan, "Control of arbitrary waveforms by means of adaptive digital feedback algorithm," *Przeglad Elektrotechniczny*, pp. 122–125, R. 80, Nr 2/2004.

Manuscript received February 26, 2004; revised August 4, 2004.